Review Paper

La-Ce doped TiO_2 nanocrystals: a review on synthesis, characterization and photocatalytic activity

A. Amritha[1] · M. Sundararajan[1] · R. G. Rejith[1] · M. A. Mohammed-Aslam[2]

Abstract
Titanium dioxide (TiO_2) is one of the best semiconductor photocatalysts due to its high stability, oxidative power, non-toxicity, low cost etc. But its photocatalytic activity is limited due to rapid recombination of photo-generated electron-hole pair, wide band gap and anatase to rutile phase transformation. These disadvantages can be eliminated by introducing dopants into the TiO_2 nanocrystals. Sol-gel and hydrothermal methods can be used for the synthesis of doped and co-doped TiO_2 nanocrystals. Advanced characterization techniques can be used for the study of phase structure, optical properties, thermal properties, surface area, morphological changes and photocatalytic activity of doped and co-doped TiO_2 nanoparticles. Doping inhibits the anatase to rutile phase transformation and suppresses the recombination of photo-generated electron-hole pair which enhances the photocatalytic activity. Here we made a review on the synthesis, characterization and photocatalytic activity of La, Ce doped and co-doped TiO_2 nanoparticles.

Keywords TiO_2 Nanocrystals · Lanthanum · Cerium · Doping · Photocatalytic activity

1 Introduction

Titanium dioxide (TiO_2) is the best semiconductor photocatalyst used for environmental remediation such as destruction of toxic organic compounds, inactivation of organisms in water and air and energy conversion process. Properties like high stability, oxidative power, non-toxicity, low cost and high photo degradation efficiency makes TiO_2 the best one [1–3]. The extent and nature of crystalline phase (anatase, rutile, brookite) determines the intrinsic properties of titaniawhich is useful in many applications [4]. Nano scale TiO_2 is used in waste water treatment, air purification, solar energy transfer and storage [5]. It is also used in optical sensors, solar devices, photoconductors, photocatalysts etc. But there are some limitations associated with TiO_2 nano crystals.

Low quantum yield due to high recombination of photo-generated electron hole pairs and little efficiency under visible light are the two main disadvantages of nano TiO_2. In TiO_2, the band gap is wide (3.2 eV). So it uses only ultra violet region of the electromagnetic spectrum. It is observed that only 3–5% of the total solar energy is used which is very low. Methods including noble metal modification, dye sensitization, compound semiconductor, metal ion doping etc. can be used to modify TiO_2 nanocrystals [5]. Doping is the most important method among these. By doping with transition metals or noble metals or rare earth metals the recombination of electron hole pairs can be reduced and also cause the absorption to shift to the visible region. The effect of La or Ce doping on TiO_2 nanoparticles is considering here. Lanthanum doped TiO_2 is better than undoped TiO_2 for the photocatalytic degradation of organic compounds because La doping increases the organic compound adsorption, thermal stability of TiO_2 and electron-hole pair separation. Sol-gel derived Ce doped TiO_2 improves the photocatalytic activity by

✉ M. Sundararajan, rajanmsundar77@yahoo.com | [1]Minerals Section, Materials Science and Technology Division, National Institute for Interdisciplinary Science and Technology (CSIR-NIIST), Council of Scientific & Industrial Research, Thiruvananthapuram, Kerala 695019, India. [2]Department of Geology, School of Earth Sciences, Central University of Karnataka, Kadaganchi, Kalaburagi, Karnataka, India.

SN Applied Sciences (2019) 1:1441 | https://doi.org/10.1007/s42452-019-1455-7

Received: 9 July 2019 / Accepted: 7 October 2019 / Published online: 19 October 2019

increasing absorption and generation of electron hole pair [6, 7]. Ce doping causes the absorption edge to shift from UV region to the visible region which can also promote the photocatalytic activity [7, 8].

To prevent the anatase to rutile transformation and to inhibit its particle growth different types of dopants can be added. Lanthanum is the most important rare earth metal used for this because it increases the thermostability of anatase phase whose photocatalytic activity is much greater than that of rutile phase [3]. Modification of nano TiO_2 by doping with non-metals will cause the absorption edge to shift to visible region and the band width will become narrow. But metal ion doping will suppress the photo-generated electron-hole pair recombination by temporarily trapping them. So it is found that nano TiO_2 can be modified effectively by co-doping (metal-metal, metal- nonmetal and nonmetal-nonmetal) [9, 10]. When La or Ce is incorporated into TiO_2, its properties will change which is summarized in Fig. 1. This article reviews the synthesis, characterization and photocatalytic activity of La, Ce doped and co-doped TiO_2.

2 Synthesis

The general methods used for the synthesis of La-Ce doped TiO_2 are (i) Sol-Gel method, (ii) Hydrothermal method.

2.1 Sol–gel method

Sol-gel process is a wet chemical technique which uses either a solution or colloidal particles to form an integrated network (gel). In sol-gel process a stable colloidal solution, called sol is formed initially. The sol is a liquid suspension of solid particles ranging from 1 nm to 1 micron. Precursors used in this process are metal alkoxides and metal chlorides. Sol is obtained by hydrolysis and partial condensation of precursors. Further condensation of sol particles into a 3 dimensional network produces a gel material. The gel is diphasic material in which solids encapsulate the solvent. The encapsulated liquid can be removed from the gel by either evaporative drying or with supercritical drying or extraction. The solid product is called xero-gel when gels are dried by evaporation. When the gels are dried by super critical drying, the dried gel is called aerogel. Sol-gel method is the most important method adopted for the synthesis of lanthanum (La) and cerium (Ce) doped TiO_2 nanocrystals. This is simple, cost effective and low temperature procedure and the synthesized nanostructure possess high purity, homogeneity and controlled morphology. Flowsheet showing the sol-gel synthesis is shown in Fig.2.

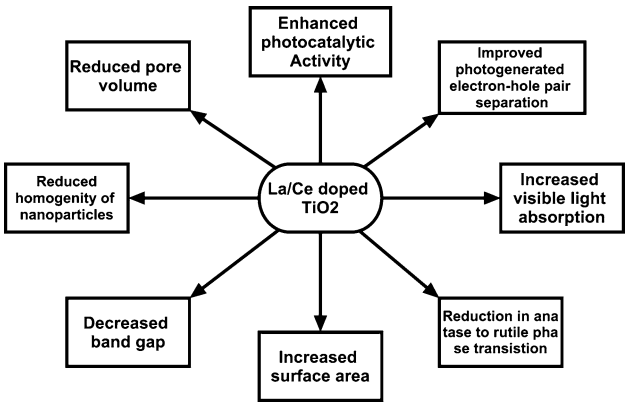

Fig. 1 Properties of La or Ce doped TiO_2

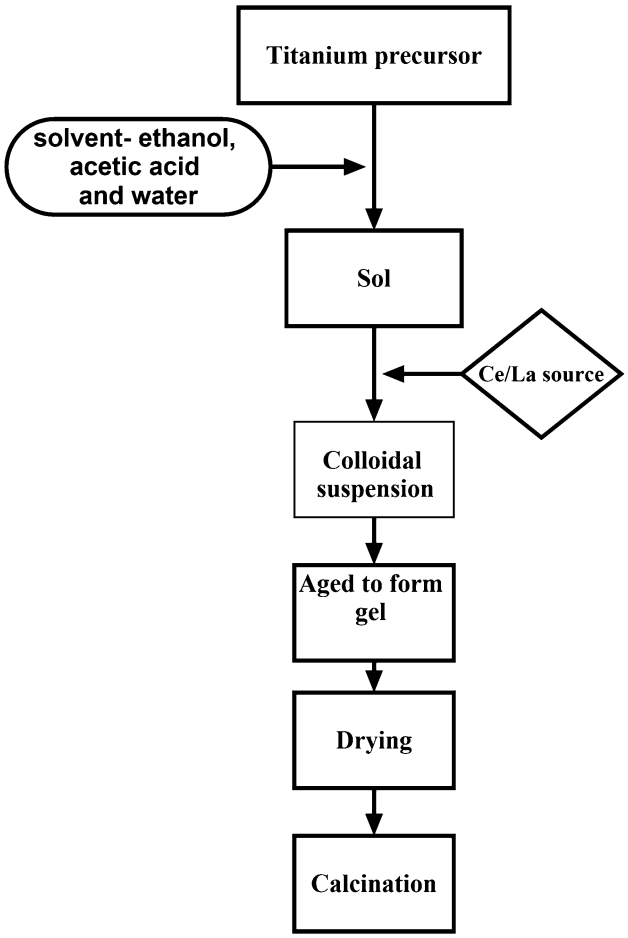

Fig. 2 Flowsheet showing the sol-gel synthesis

In this method, a required amount of titanium precursor, titanium alkoxide (usually titanium isopropoxide or tetrabutoxytitanium (TBOT)) is dissolved in absolute ethanol. This is further mixed with a solution containing water, ethanol and acetic acid. To the above sol, lanthanum nitrate or cerium nitrate solution is added to get

Table 1 Conditions involved in Sol-Gel method (La)

Ti precursor	Solvent	P^H	La source	Aging condition	Drying condition	Calcination condition	References
$Ti(O\text{-}Bu)_4$	Ethanol	7	$La(NO_3)_3{\cdot}6H_2O$	24 h	70 °C and 120 °C (12 h)	500 °C and 800 °C (4 h)	[7]
$Ti(O\text{-}Bu)_4$	Ethanol & Acetic acid	–	$La(NO_3)_3{\cdot}6H_2O$	–	–	500 °C	[1]
$Ti(O\text{-}Bu)_4$	Ethanol	1-2	$La(NO_3)_3{\cdot}6H_2O$	–	60 °C (24 h)	At different temperature (4 h)	[33]
$Ti(O\text{-}Bu)_4$	Isobutanol	3	$La(NO_3)_3{\cdot}6H_2O$	–	40 °C (3 days), 60 °C (2 days), 120 °C (1 day)	450 °C (5 h)	[4]
$Ti(O\text{-}Bu)_4$	Ethanol and Acetic acid	–	$La(NO_3)_3{\cdot}6H_2O$	Several hours	80 °C (4 h)	360 °C, 450 °C, 600 °C (2 h)	[3]
$Ti(O\text{-}Bu)_4$	Ethanol and Acetic acid	–	$La(NO_3)_3$	2 days	80 °C	500 °C (2 h)	[6]
$Ti(O\text{-}Bu)_4$	Ethanol and Acetic acid	–	$La(NO_3)_3$	–	100 °C (12 h)	500 °C (4 h)	[25]

Table 2 Conditions involved in Sol-Gel method (Ce)

Ti precursor	Solvent	Ce source	Aging condition	Drying condition	Calcination condition	References
Titanium is opropoxide	Ethanol and Glacial acetic acid	Cerium nitrate	24 h	–	400 °C (4 h)	[34]
$Ti(O\text{-}Bu)_4$	Ethanol and Acetic acid	Ammonium cerium nitrate	12 h	70 °C (5 h)	550 °C (4 h)	[20]
Titanium isopropoxide	1-propanol water mixture	Ceric ammonium nitrate	–	100 °C	400 °C and 600 °C	[35]
Titanium isopropoxide	2-Propanol	$Ce(NO_3)_3{\cdot}6H_2O$	10–12 h	80 °C	450 °C (4 h)	[36]

Table 3 conditions involved in sol-gel synthesis of Ce co-doped TiO_2

Co-dopant	Ti source	Ce source	Co-dopant precursor	Solvent	Aging condition	Drying condition	Calcination condition	References
Boron	Tetrabutyl titanate and Titanoustrichloride	$Ce(NO_3)_3.6H_2O$	Boric acid	Ethanol	2 days	100 °C	300 °C,500 °C,700 °C or 900 °C (5 h)	[37]
Nitrogen	Tetra butyl titanate	$Ce(NO_3)_3.6H_2O$	Urea	Ethanol	–	110 °C (8 h)	500 °C (2 h)	[38]
Iodine	Tetra butyl titanate	Cerous nitrate	Iodic Acid	n-Butanol	–	80 °C	400 °C and 500 °C	[14]
Copper	TiO_2slurry	$Ce(NO_3)_4$	$Cu(NO_3)_2$	–	24 h	100 °C (1 h)	500 °C (2 h)	[15]
Carbon	$Ti(O\text{-}Bu)_4$	$(NH_4)_2Ce_2(NO_3)_6$	Glucose	Isopropanol	–	60 °C (vacuum)	–	[16]
Nitrogen	$Ti(O\text{-}Bu)_4$	Cerium nitrate	Ammonium nitrate	Ethanol and Glacial acetic acid	48 h	80 °C (12 h)	–	[9]
Sulphur	$Ti(O\text{-}Bu)_4$	$Ce(NO_3)_3{\cdot}6H_2O$	Thio urea	Ethanol	12 h	80 °C (10 h)	550 °C (2 h)	[10]
Silicon	$Ti(O\text{-}Bu)_4$	$Ce(NO_3)_3{\cdot}6H_2O$	Tetra ethyl orthosilicate	Acetic acid	–	110 °C (12 h)	Various temperature	[23]

a colloidal suspension. The colloidal suspension thus obtained is stirred well and aged to form gel and the gel is dried in vacuum. The product thus obtained is calcined at a temperature in the range 400–800 ℃ [1]. Different conditions involved in the sol-gel synthesis of La and Ce doped TiO_2 nanocrystals are summarized in Tables 1 and

Table 4 Conditions involved in the sol-gel synthesis of La co-doped TiO_2

Co-dopant	Ti source	La source	Co-dopant source	solvent	Aging condition	Drying condition	Calcination condition	References
Tin	$Ti(O\text{-}Bu)_4$	$La(NO_3{\cdot}6H_2O$	$SnCl_4{\cdot}5H_2O$	Ethanol and Acetic acid	Several hours	80 °C (12 h)	360 °C, 450 °C, 600 °C (2 h)	[3]
Nitrogen	$Ti(O\text{-}Bu)_4$	$La(NO_3)_3{\cdot}6H_2O$	Urea	Ethanol and Acetic acid	48 h	–	500 °C (3 h)	[38]
Sodium	$Ti(O\text{-}Bu)_4$	$La(NO_3)_3{\cdot}6H_2O$	Sodium nitrate	Methyl cellosolve	–	–	450 °C (1 h)	[39]
Tungston	$Ti(O\text{-}Bu)_4$	$La(NO_3)_3{\cdot}6H_2O$	$(NH_4)_{10}W_{12}O_{41}$	Ethanol and Acetic acid	5 h	100 °C (6 h)	400 °C (3 h)	[40]
Iodine	$Ti(O\text{-}Bu)_4$	$La(NO_3)_3{\cdot}6H_2O$	Iodic acid	n-Butanol	–	80 °C	400 °C, 500 °C, 600 °C (2 h)	[31]
Europium	$Ti(O\text{-}Bu)_4$	$La(NO_3)_3$	$Eu(NO_3)_3$	Ethanol and Acetic acid	24 h	60 °C	Different temperature (3 h)	[18]
Boron	$Ti(O\text{-}Bu)_4$	$La(NO_3)_3$	Boric acid	Ethanol	1 h	60 °C (16 h)	400 °C (3 h)	[22]

2 respectively. Same method can be used for the synthesis of La and Ce co-doped TiO_2 nanoparticles. Different conditions involved in the sol-gel synthesis of Ce and La co-doped TiO_2 are explained in Tables 3 and 4 respectively.

2.2 Hydrothermal method

Hydrothermal or solvothermal is the most common and widely used method for the synthesis of nanomaterials with various morphologies. Here the reactants are placed in an autoclave which is filled with water or organic compounds and the reaction is carried out under high temperature and pressure conditions. If water is used as the reaction medium, then it is called hydrothermal method and if non-aqueous solvents are used, then the method is called solvothermal. There are different types of autoclaves with different functions. Generally, Teflon-lined autoclaves are used for obtaining high temperature and pressure conditions. It maintains alkaline media and exhibit strong resistance to hydrochloric acid compared to glass and quartz autoclaves. Therefore Teflon-lined autoclaves are more preferred for performing reactions under desired conditions. This method can increase the reaction between reactants and promote hydrolysis which is then followed by crystal growth resulting in self assembly of nanomaterials in the solution. The properties, morphology, size and structure of the nanomaterials can be changed by varying the reaction parameters like reaction time, temperature, pH, concentration of the reactants etc. That is this method can be used for the synthesis of nanomaterials with variety of shapes compared to other methods. Hydrothermal method can be used for the synthesis of La and Ce doped and co-doped TiO_2 nanoparticles. Flowsheet showing hydrothermal synthesis is shown in Fig. 3.

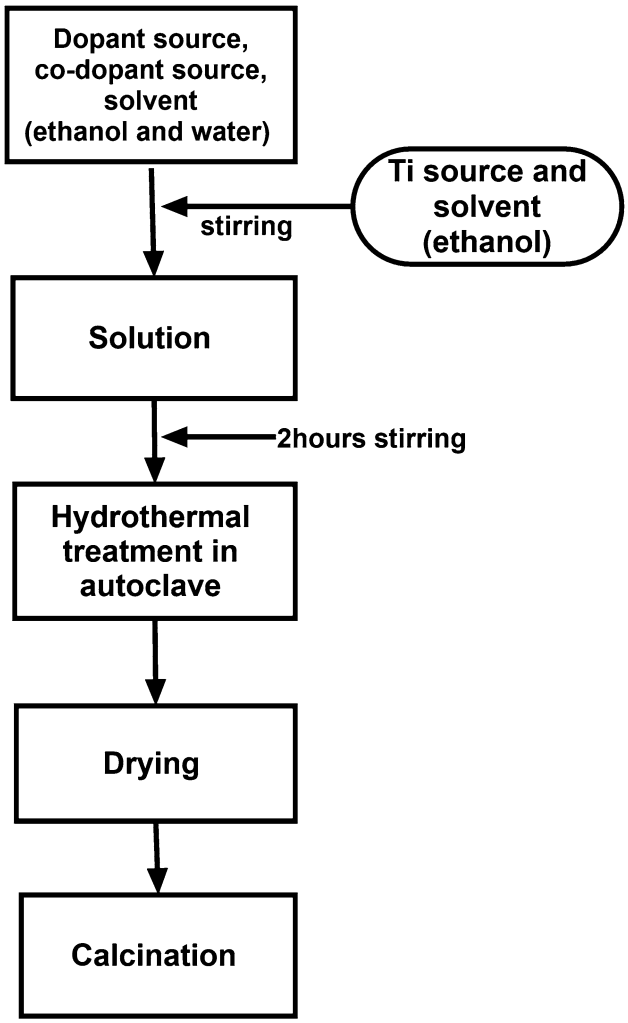

Fig. 3 Flowsheet showing hydrothermal synthesis

Table 5 Conditions involved in hydrothermal synthesis of La and Ce doped and co-doped TiO_2

Dopant	Co-dopant	Ti source	Dopant source	Co-dopant source	Hydrothermal treatment	Drying condition	Calcination condition	References
Cerium	Nitrogen	$Ti(O\text{-}Bu)_4$	$La(NO_3)_3{\cdot}6H_2O$	Urea	120 °C (16 h)	100 °C (over night)	450 °C (3 h)	[27]
Lanthanum	Carbon	$Ti(SO_4)$	$La(NO_3)_3{\cdot}NH_2O$	Glucose	180 °C (12 h)	–	–	[17]
Lanthanum	Nitrogen	$Ti(O\text{-}Bu)_4$	$LaCl_3{\cdot}nH_2O$	Triethyl amine	180 °C(12 h)	–	–	[21]
Lanthanum	Carbon	$Ti(O\text{-}Bu)_4$	La_2o_3	Ethyl alcohol	180 °C (6 h)	–	–	[41]

It is observed that if Ce^{4+} is incorporated into TiO_2 nanocrystals by the hydrothermal method, it will improve the photocatalytic activity of nano TiO_2 under both ultraviolet and visible irradiation. It is due to the 4f electron configuration of Ce^{4+} ions which is responsible for interfacial charge transfer and elimination of electron hole pair combination [2].

Conditions involved in the hydrothermal synthesis of La and Ce doped and co-doped TiO_2 nanoparticles are summarized in Table 5.

3 Characterization of nanocrystals

The advanced material characterisation techniques like X-ray diffraction (XRD), X-ray photoelectron spectroscopy (XPS), UV-Visible, Fourier-transform infrared spectroscopy (FTIR), Thermogravimetry/Differential Thermal Analysis (TG-DTA), Brunaeur-Emmet-Teller surface area analysis (BET), Scanning electron microscope (SEM) and Photoluminescence (PL) are used.

3.1 Phase structure and chemistry

XRD helps us to identify the crystal phase and determine the anatase torutile ratio as well as the crystallite size of each phase present. In the TiO_2 spectra, the XRD peaks at $2\theta = 25.25(101)$ and 48° corresponds to the crystal of anatase form and peaks at $2\theta = 27.42(110)$ and 54.5° can be identified as the crystal of rutile form. From XRD analysis, it can be concluded that TiO_2 and La doped TiO_2 is composed of anatase and rutile phases [11]. The diffraction patternin both TiO_2 and La doped TiO_2 is similar. Peaks corresponding to the formation of metal oxides such as La_2O_3 are not found in La doped TiO_2. There is also an observation that for La doped TiO_2 the peak at $2\theta = 25.4°$ is slightly shifted to a lower angle. This is due to the substitution of La^{3+} ionsof larger radius (1.15 Å) in TiO_2 lattice for small radius Ti^{4+} (0.745 Å) which cause distortion of La doped TiO_2 lattice. There is also an observation that in La doped TiO_2 the crystal size decreases with an increase in La content and the crystal size is less than that of pure TiO_2. This may arise from the incorporation of La into TiO_2 which cause a decrease in grains growth. In comparison with the standard values of bulk TiO_2, the lattice parameters of La doped TiO_2 is smaller. The difference indicates the successful incorporation of La^{3+} ions into the TiO_2 lattice. Since the ionic radius of La^{3+} ions is higher than that of Ti^{4+}, it interstitially substitute Ti^{4+} ion sites Anandan et al. [1]. The comparison of the XRD spectrum of pure TiO_2 and La doped TiO_2 reveals that for pure TiO_2 when the calcining temperature is 600 °C, rulite phase start to appear and when the calcining temperature is 700 °C, anatase phase is disappeared. But for La doped TiO_2 a little rutile phase appears when the calcining temperature is 700 °C and even when the calcining temperature is 800 °C most of the phase is still anatase. That is, the doping of La to TiO_2 reduces the phase transformation from anatase to rutile and increase the starting temperature of phase transformation [11]. The XRD patterns of La and Co co-doped TiO_2 reveals that with increase in La content, crystal size decreases. Since La is doped into TiO_2 lattice there is no peaks corresponding to lanthanum oxides [17]. One important factor which determines the photocatalytic activity of titania is its crystalline phase and it is found that anatase phase is more active than rutile phase in photocatalytic degradation of organic compounds. In La, Eu co-doped TiO_2, the XRD patterns shows anatase phase. As the calcination temperature increases from 400 to 900 °C, the anatase peak intensity increases and the width of (101) plane decreases. After 900 °C anatase to rutile phase transformation begins and rutile phase appears slightly but anatase phase is dominant [18].

XRD studies indicate that Ce doping inhibit anatase to rutile phase transformation in TiO_2 nanoparticles. Since the ionic radii of Ce^{4+} (0.093 nm) and Ce^{3+} (0.103 nm) is larger than that of Ti^3 (0.064 nm), the doping of Ce into TiO_2 lattice cause lattice distortion and expansion and deposition of strain energy in the crystal. The result is that the anatase to rutile phase transition is reduced and the transition temperature is increased [12]. Larger ionic radii of Ce^{3+} and Ce^{4+} ions than that of Ti^{4+} make their doping into TiO_2 lattice difficult. As a result, a few ions are penetrated into the lattice and most of them are distributed on the surface.

These generate a grain boundary that separate nanoparticles and inhibit their growth. This reduction in size increases with an increase in Ce content which is responsible for the main peak (101) reduction [13]. XRD can also be used for the identification of crystal phase and determination of crystallite size of La and Ceco-doped TiO_2 nano particles. Ce/N co-doped TiO_2 nanoparticles calcined at 400 °C exhibit only anatase phase. Due to the incomplete crystallization, the X-ray diffraction peaks of the sample are wide. The anatase diffraction peaks are sharp and intense for the sample calcined at 600 °C which indicate that most of the sample is in the anatase phase. Weak rutile diffraction peaks are also appeared at 600 °C due to the presence of trace amounts of the rutile phase in the sample. If the calcination temperature is 700 °C, rutile diffraction peaks become sharp and intense which indicates that most of the sample is in rutile phase. XRD does not give characteristic diffraction peaks of cerium and nitrogen since the amount of Ce and La are below the detection limit of this technique. It is also found that peak which depends on the crystalline size. As the size of the particles decrease, peaks become wider [12]. In Ce /I co-doped TiO_2calcined at 400 °C and 500 °C only anatase phase is detected. But in I doped TiO_2 there is 40% contribution from rutile phase which indicates that Ce doping into I doped TiO_2 lowers anatase to rutile transition and hence stabilize anatase phase. The measured surface area of Ce/I-TiO_2 at 400 °C and 500 °C are 149 m^2/g and 129 m^2/g respectively. That is as the calcination temperature increases surface area decreases. As a result, less active surface sites are exposed to targeted reactants [14]. The Cu diffraction peaks at $2\theta = 43.3°$ and $2\theta = 52°$ are observed for both Cu/Ce co-doped TiO_2 and Ce/Cu co-doped TiO_2. This indicates that Cu is well dispersed on the surface of TiO_2. Due to the successful reduction of CuO, no CuO diffraction peak is found at $2\theta = 35.6°$. There is a peak at $2\theta = 28°$ in both Cu/Ce co-doped TiO_2 and Ce/Cu co-doped TiO_2resulting from the presence of CeO_2 phase [15]. The XRD of undoped titania exhibit a strong (101) anatase peak at $2\theta = 25.4°$. In addition to this, there is a small brookite phase (121) at 30.1° in undoped titania. But in both doped and co-doped samples onlyanatase phase is there. The decrease in intensity of the peak in carbon doped and co-doped samples arise from the shield effect of doped carbon species. In Ce–C co-dopedtitania, there is no peak corresponding to Ce which indicates that it is difficult for Ce^{4+} to enter into TiO_2 lattice since it is larger than Ti^{4+} [16]. The XRD results of Ce-S co-doped TiO_2 shows only anatase type peaks and there is no evidence for the presence of other polymorph for TiO_2 likerutile or brookite. Peaks corresponding to the presence of CeO_2 and Ce_2O_3 are absent in the spectra. This indicates that either the amount of Ce is very small in the sample or it is well dispersed through channel walls. As the cerium content in the sample increases the intensity of anatase peak and crystal size decreases. Presence of Ce-O-Ti on the surface of the catalyst is responsible for the reduction in crystal size [10].

3.2 Optical properties

UV-Visible spectrum of La^{3+} doped nano TiO_2 shows a shift in absorption band to longer wavelength region and also there is an increase in the rate of absorption of light. For La doped TiO_2 absorption is in the visible region (420–700 nm) but for pure TiO_2 it is in the ultra violet region (378 nm). This shift is due to the larger radius of La^{3+} (0.115 nm) than that of Ti^{4+} (0.068 nm). Thus it is difficult for La^{3+} to enter into the lattice of nano TiO_2. La that covers the surface of TiO_2 is in its oxide form when the amount of La dopant is small. This reduces the grain size. As a result, the size of La doped TiO_2 is much smaller than that of undoped TiO_2. Elements that cover the surface of nano TiO_2 can absorb light over a wide range and this energy is transferred to nano TiO_2. This improve the photocatalytic activity Guan et al. [5]. In pure TiO_2 excitation of oxygen 2p electrons to titanium 3d level is responsible for the absorption in the ultra violet region. The charge transfer between the valance or conduction band of TiO_2 and Lanthanum 4f level is the reason for the red shift observed in the absorption spectra of La doped TiO_2 and trapping levels in La doped TiO_2 decreases the band gap of TiO_2. Fig. 4 explains the proposed photocatalytic mechanism of both doped and undoped TiO_2. La ions in the doped TiO_2 increase its visible light absorption ability Yao et al. [19]. In pure TiO_2, the absorption is in the range of 200 to 380 nm. In Ce doped TiO_2, the absorption is shifted to the visible region. The dependence of optical absorption with dopant ion is due to the penetration of photons into the TiO_2 nanoparticles [20]. It is observed that La/N co-doping reduces the band gap from 3.18 to 2.84 eV. Nitrogen doping introduces an impurity level near the valence band edge which causes the absorption band to shift to visible region in N doped TiO_2. La doping reduces the formation of recombination centers developed by N doping and also it induces an impurity energy level below the conduction band of TiO_2. Hence there are two impurity levels in La/N co-doped TiO_2 and three possible electronic transitions. The transitions from valence band of TiO_2 to La impurity level, N impurity level to La impurity level and N impurity level to conduction band of TiO_2 increases the number of photo-generated electron-hole pair. Therefore, La/N co-doped TiO_2 shows enhanced visible light absorption capacity [21]. In La/Eu co-doped TiO_2, the absorption peak is shifted to visible region. This red shift can be attributed to the transitions of 4f electrons of Eu^{3+} and La^{3+} [18]. Similarly in La/B co-doped TiO_2, absorption is shifted to

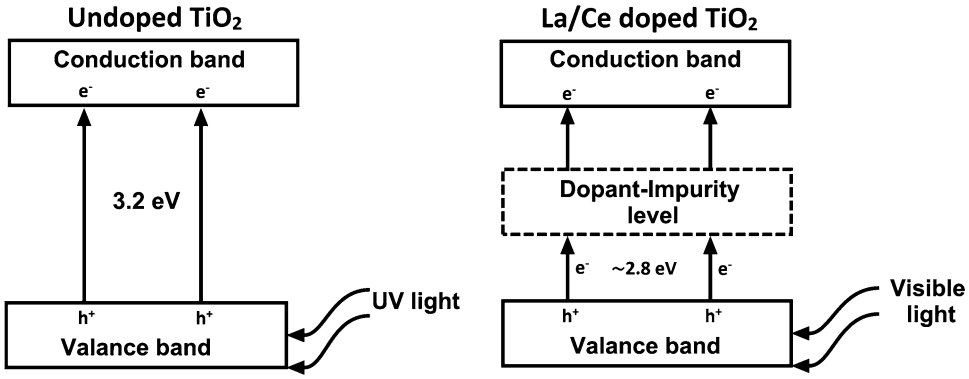

Fig. 4 Proposed photocatalytic mechanism of undoped and doped TiO_2

visible region and the band gap is found to be 2.80 eV which is lower than that of pure TiO_2 (3.18 eV), La doped TiO_2 (2.87 eV) and B doped TiO_2 (2.89 eV) [22]. In Ce/N co-doped TiO_2, the absorption band is shifted to visible region and the energy gap is found to be 2.52 eV which is lower than that in pure and singly doped TiO_2. In N doped TiO_2, nitrogen substitute oxygen from lattice sites to form nitride (Ti-N). This is responsible for the observed red shift. The Yellow Cerium oxide formed during calcination can absorb ultra violet light in Ce doped TiO_2. Ce generates 4f orbital energy level below the conduction band of TiO_2. Under visible light irradiation, the valence band electrons of Ce doped TiO_2 and the ground state electrons of Ce_2O_3 can be excited to the Ce 4f orbital energy level which leads to red shift [12]. It is found that absorption is shifted to visible region in Ce-Si co-doped TiO_2. As the cerium content increases, the absorption also increases which lies in the range of 400–550 nm. If Si content is increased by keeping Ce content constant, it is observed that absorption is shifted to shorted wavelength due to quantum size effect of semiconductors. Addition of Ce enhances red shift and hence improves photocatalytic activity [23].

The XPS spectrum of Ti 2p of TiO_2 is a single, well-defined, spin-split doublet in which the separation between two peaks is 6 eV. This can be attributed to Ti^{4+} in a tetragonal structure. The binding energies of the peaks are 464.8 eV for Ti $2p_{1/2}$and 459 eV for Ti $2p_{3/2}$. The XPS spectrum of Ti 2p in La doped TiO_2 is similar to that of undoped TiO_2. In La doped TiO_2, La^{3+} ions doped into TiO_2 lattice interact with oxidic sites of TiO_2 which gives a broadened spectrum of La 3d [1]. The XPS spectra of La 3d concludes that La exists in +3 state in La doped TiO_2 and the binding energies of the peaks are 835, 844 and 852 eV. Compared to the La 3d spectrum of pure La_2O_3, peaks in the XPS spectrum of La doped TiO_2 are shifted to the low binding energy. This chemical shift is due to the change in the chemical environment of La^{3+} and difference in distance between lanthanum and oxygen compare to pure La_2O_3. The Ce 3d spectrum of Ce doped TiO_2 shows peaks with binding energies 873 eV and 895 eV respectively. That is there may be no change in the oxidation state of ions as a result of doping [24]. The characteristic vibration of O-H give absorption bands at 3414 cm-1 and 1635 cm-1 in the FTIR spectrum of La doped TiO_2. This indicates that more H_2O molecules are get absorbed on the surface of La doped TiO_2. As a result, more hydroxyl radicals are generated from the surface after irradiation. Another absorption band observed at 530 cm^{-1} is due to the characteristic vibration of Ti-O-Ti [25]. The absorption band at 1635 cm^{-1} is due to the bending vibrations of –OH groups and the broad peak at 3414 cm^{-1} is contributed by surface adsorbed hydroxyl groups. In addition to this, surface adsorbed water molecules give sharp peaks in the range 2750-3000 cm^{-1}. In the case of undoped TiO_2, intensity of absorption bands at 3414 cm^{-1} and 2750-3000 cm^{-1} are decreased after heat treatment at 900 °C. This is due to the removal of terminal hydroxyl groups. But in the case of La doped TiO_2, these bands are intense even after heating at 900 °C. This indicates that lanthanum doping introduce more hydroxyl groups on the surface of TiO_2. Since La is in +3 oxidation state in order to maintain electrical neutrality more hydroxide ions are adsorbed on the surface of TiO_2. These hydroxide ions are reduced by photo-generated halls to form hydroxyl radicals and the adsorbed molecules are get oxidised. This charge imbalance is not present in the case of Ce doped TiO_2 and hence less hydroxyl groups are get adsorbed on the surface [26].

The FTIR spectrum of Ce/N co-doped TiO_2 exhibits three regions. In the first region observed between 3000 and 3500 cm^{-1} there are two peaks. The peaks at 3422 cm^{-1} are attributed to the O–H group stretching vibration of surface adsorbed water molecules and the second peak at 3186 cm^{-1} result from the N-H stretching vibrations. In the second region 1200-1800 cm^{-1}, there is a peak at 1622 cm^{-1} due to -OH bending vibrations and another one at 1391 cm^{-1} due to -NO_x. The third region 500–1000 cm^{-1} can be attributed to Ti–O stretching vibrations [27]. In the case of Ce/S co-doped TiO_2 the stretching and bending vibrations of surface adsorbed hydroxyl groups and water molecules give peaks at 3423 cm^{-1} and 1628 cm^{-1}. The

peaks below 900 cm^{-1} can be attributed to stretching vibrations of Ti–O bonds [10].

PL spectra of La-Sn co-doped TiO_2 has minimum intensity compared to that of pure TiO_2, La doped TiO_2 and Sn doped TiO_2. That is, in co-doped TiO_2, recombination rate of photo-generated pair is minimum and separation rate is maximum. This increased separation rate is favourable for photocatalytic activity [3]. The intensity of PL spectra of La/B co-doped TiO_2 is low compared to pure and singly doped TiO_2. This is due to effective separation of photo-generated electron-hole pair [22]. The PL spectra of Ce/N co-doped TiO_2 have two peaks, one at 369 nm due to the band gap transition and the second one at 470 nm corresponding to charge carrier transition. There is a small shift to short wavelength due to the incorporation of cerium. Cerium doping also cause reduction in the peak intensity due to the suppression of electron-hole pair recombination and reduction of recombination centers. There is an increase in peak intensity if the Ce content increases beyond a limit because the excess Ce will generate more recombination centres [27]. In Ce/S co-doped TiO_2, the intensity of PL spectra is less than that of pure TiO_2 and singly doped TiO_2. This is because incorporated Ce generates trap sites on the surface which suppress the recombination of photo-generated electron-hole pair. But excess addition will enhance the recombination of photo-generated charge carriers [10].

3.3 Thermal properties

TG curve of La doped TiO_2 consist of three steps of weight loss. Evaporation of physically absorbed water molecules is responsible for the first step while the second step results from the combustion of organic compounds (a total 21% weight loss at the temperature range from room temperature to 450 °C). Dehydroxylation of gel is responsible for third step weight loss (450 °C to higher temperature). The DTA curve peak observed at 100 °C corresponds to desorption of water and ethanol in the gel and that at 350 °C results from the decomposition of organic matters. In pure TiO_2, exothermic peak at 578 °C observed in the DTA curve results from the phase transformation from anatase to rutile phase. But in La doped TiO_2, the exothermic peak corresponding to phase transformation is observed at 600 °C. This indicates that La doping suppresses phase transformation of TiO_2 which is in agreement with XRD data [3, 11]. The TG curve of La/Sn co-doped TiO_2 shows three step weight loss in which the first step results from the evaporation of physically absorbed water, the second step can be attributed to the combustion of organic compounds and the third step derives from the dehydroxylation of gel. The DTA curve of La-Sn co-doped TiO_2 shows an exothermic peak at 590 °C corresponding to anatase to rutile phase transformation which is found to be greater than that of pure TiO_2 (578 °C) [3].

In DTA curve of Ce doped TiO_2, there is a small endothermic peak below 100 °C resulting from desorption of water and the small peaks at 120 ℃ and 225 °C arises from the combustion decomposition of organic matters. In between 250 °C and 359 °C, there is a sharp endothermic reaction peak which represents the phase transformation of the powder from amorphous to anatase phase. It is observed that the crystallization temperature is decreased with increase in cerium content. The TG curve of Ce doped TiO_2 shows three step weight loss. The first weight loss observed at temperatures below 100 °C is due to the evaporation of water molecules from the powder and the second weight loss resulting from the removal of chemisorbed water molecules and release of organic residues occurs at temperatures between 120 and 350 °C. Removal of –OH groups is responsible for the third weight loss from 380 to 600 °C. Approximately 20% of weight loss is there in total [20]. The DTA curve of Ce/N co-doped TiO_2 shows an endothermic peak in the range 163–201 °C due to the loss of adsorbed water molecules and initial decomposition of urea. Between 201 and 308 °C, there is a sharp and narrow endothermic peak resulting from the decomposition of urea and cerium nitrate completely. Due to the structure change of amorphous precursor to anatase TiO_2, there are several small exothermic peaks in the range 370–420 °C. There is an exothermic peak between 551 and 612 °C resulting from the anatase to rutile phase transition [12].

3.4 Surface area and morphological change

BET surface area studies reveals that both TiO_2 and La or Ce doped TiO_2have pore diameter between 3.5 and 10 nm. It is observed that surface area increases with the quantity of dopant (La or Ce) and in the case of La doped TiO_2 the highest surface area is obtained when the amount of La^{3+} is 0.5 wt%. This surface area is equal to three times the value of undoped TiO_2. High dispersion and the higher ionic radii of La^{3+} and Ce^{3+} than Ti^{4+} is responsible for the increase in surface area. For La^{3+}, ionic radius is 1.15 Å and for Ce^{3+} 1.03 Å. When La or Ce is substituted on TiO_2 lattice (anatase structure), the Ti-O-La or Ti-O-Ce bond is formed to modify the structural arrangement and hence BET surface area. BET studies show that the surface area of 0.5 wt% La or Ce doped TiO_2 treated at 800 °C decreases in comparison with those treated at 500 °C. This phenomenon can be explained on the basis of growth in crystal size and starting of the sintering process. It is observed that during heat treatment coalescence of pores takes place which results in an increase in pore diameter and hence reduction in pore volume [7]. It is found that the BET surface area of La/Eu co-doped TiO_2 (83–95 m^2/g) is greater than that of pure TiO_2

(30.3 m^2/g). This high surface area improves the absorption ability of TiO_2 frame works. It is found that the linkage between rare earth ions and titanium by oxygen-bridge is responsible for this enhanced surface area [18]. The BET surface area of La/Sn co-doped TiO_2 is determined to be 85.7 m^2/g which is higher than that of pure TiO_2 (4.4 m^2/g) [3]. This high surface area is responsible for the enhanced photocatalytic activity. The enhanced surface area of La/ B co-doped TiO_2 nanoparticles (94.66 m^2/g) provides more active sites which is favourable for photocatalytic activity [22] . The BET surface area studies reveal that incorporation of Ce into N-TiO_2 increase the surface area. The measured surface area of Ce/N co-doped TiO_2 is 152.82 m^2/g. Decrease in particle size is responsible for the increased surface area [27]. The BET surface area of Ce/S co-doped TiO_2 is greater than that of pure TiO_2, S doped TiO_2, Ce doped TiO_2. In addition to this, there is a decrease in pore size due to decrease in particle size [10].

The SEM analysis of Ce doped TiO_2reveals that as the amount of Ce doped in TiO_2 nanoparticles increases, reduction in size occurs which causes homogeneity of the nanoparticles to decrease [28]. Due to this size shrinkage inter molecular and inter atomic forces of attraction become strong. This powerful attraction force is responsible for the greater tendency of nanoparticles to come close to each other and they agglomerate. In addition to the reduction in crystal growth, the anatase to rutile phase transition is suppressed when CeO is doped into TiO_2 nanocrystals. This is due to the presence of Ce–O–Ti bonds [20]. SEM images of both un-doped TiO_2 and La doped TiO_2 exhibit partial crystalline nature which indicatesthat doping does not change the morphology of the material. That is both doped and un-doped materials have amorphous nature with rough surfaces [29]. The SEM images of La/Sn co-doped TiO_2 exhibit relative uniform particles distribution. The particles have smaller size which is responsible for the effective utilization of light source [3]. The SEM analysis of La/Eu co-doped TiO_2 shows a relative uniform particle distribution in which the diameter of particles may be in the range of 40-60 nm [18]. SEM analysis reveals that in Ce/C co-doped TiO_2 spheroidal shaped particles are distributed on a support and the particle is size is 5-10 nm which slightly larger than that obtained from XRD calculation. This indicates that during synthesis aggregation has been occurred [16].

4 Photocatalytic activity

The photocatalytic activity of La doped TiO_2 is checked by studying the degradation of monocrotophos (MCP). The results are compared with the standard degradation results of La doped ZnO photocatalysts. It is found that La doped TiO_2photocatalysts are much more active and for the light of wavelength 254 nm and 365 nm its rate constants is 1.75 and 1.125 times higher than that of La doped ZnOphotocatalysts. Small particle size, high surface area, high surface roughness, higher photonic efficiency and reduction of photogenerated electron-hole pair recombination are responsible for the high photocatalytic activity of La doped TiO_2 for the removal of MCP than other photocatalys [1]. The photocatalytic activity of Sn/La co-doped TiO_2 is evaluated by considering the degradation of RhodamineB (RhB) under UV light. For pure TiO_2 photocatalytic activity depends on calcination temperature and the best degradation is observed at 450 °C. Sn and La doping improves the photocatalytic activity and it is found that the highest degradation rate is observed for Sn/La co-doped TiO_2. The increase in photocatalytic activity due to co-doping can be attributed to increased surface area, presence of more surface hydroxyl groups and the reduction of photo-generated electron hole pair recombination [3]. It is found that the La/I co-doped TiO_2 show high visible lightphotocatalytic activity which can be explained by considering the photocatalytic degradation of oxalic acid in aqueous solution. I^{5+} ions substitute Ti^{4+} ions from TiO_2 lattice and this determines the photocatalytic activity in the visible light range. Dopant La is deposited on the surface in the form of La_2O_3 which suppresses the recombination of electron hole pair [32].

The determination of photocatalytic activity of Ce doped TiO_2 can be carried out by considering the photodegradationof Rhodamine B aqueous solution. It is found that Ce^{4+} doping improves the photocatalytic activity of TiO_2. Reason for this improved photocatalytic activity is the 4f electron configuration of Ce^{4+}/Ce^{3+}which plays an important role in separation of photo-generated electron-hole pair and interfacial charge transfer. Valance band electrons of Ce-TiO_2 and ground state electrons of Ce_2O_3 are getting excited to Ce 4f level under UV irradiation which is further transferred into adsorbed oxygen to form super oxide anion radicals. This improves photocatalytic activity [30]. The photocatalytic activity of C/Ce co-doped TiO_2 is determined by considering the photodegradation of an aqueous solution of a dye Reactive Brilliant Red X-3B under visible light irradiation. It is found that recombination of photo generated electron hole pairs is reduced when Ce is doped into the TiO_2. As a result, the photocatalytic activity of Ce/C co-doped TiO_2 is increased compared to C-doped, Ce-doped and undoped TiO_2 for the degradation of the dye [16]. The photocatalytic activity studies of Ce/S co-doped TiO_2 for degradation of an aqueous solution of dye Acid orange-7 (AO-7) reveals that the co-doped TiO_2 has an enhanced photocatalytic activity than the undoped one. Properties like increased surface area, decreased particle size, increase in the surface hydroxyl

groups and the reduction of photo-generated electron hole pair recombination are responsible for the enhanced photocatalytic activity of Ce and S co-doped TiO_2 [10]. For evaluating the photocatalytic activity of Nd/Ce co-doped TiO_2, an aqueous solution of methylene blue is taken as pollutant solution for degradation. It is found that there is an enhancement in the photocatalytic activity due to the same reasons mentioned above. It is also observed that the photocatalytic activity is decreased at higher doping levels. This is because the excessive Nd, Ce particles may occupy the active sites of photocatalyst which decreases the charge transfer from TiO_2 catalyst to methylene blue molecule. This retards photocatalytic activity [31].

5 Conclusion

TiO_2 is the best semiconductor photocatalyst used for environmental remediation such as destruction of toxic organic compounds, inactivation of organisms in water, air, and energy conversion process due to its high stability, oxidative power, non-toxicity, low cost and high photodegradation efficiency. There will be an effective change in the structure, morphology, thermal and optical properties of TiO_2 nanoparticles when dopants areintroduced into the lattice. XRD studies indicates that introduction of dopants into TiO_2 reduce anatase to rutile phase transformation. The photocatalytic activity of La, Ce doped and co-doped TiO_2 nanocrystals is enhanced due to the suppression of photogenerated electron-hole pair recombination and narrowing of band width. The absorption edge is shifted to visible region as a result of doping. This article provides an idea about the synthesis, characterization and photocatalytic activity of La, Ce doped and co-doped TiO_2 nanoparticles.

Acknowledgements The authors thank the Director, CSIR-National Institute for Interdisciplinary Science and Technology (CSIR-NIIST), Trivandrum, Kerala, India for extending the laboratory facilities.

Complaince with ethical standards

Conflict of interest The authors declare that they have no conflict of interest.

References

1. Anandan S, Ikuma Y, Murugesan V (2012) Highly active rare-earth-metal La-doped photocatalysts: fabrication, characterization, and their photocatalytic activity. Int J Photoenergy 2012:1–10
2. Liu H, Yu L, Chen W, Li Y (2012) The progress of TiO_2 nanocrystals doped with rare earth ions. J Nanomater 2012:1–9
3. Zhu X, Pei L, Zhu R, Jiao Y, Tang R, Feng W (2018) Preparation and characterization of Sn/La co-doped TiO_2 nanomaterials and their phase transformation and photocatalytic activity. Sci Rep 8(1):12387
4. Milanovic M, Nikolic LM (2014) Modification of TiO_2 nanoparticles through lanthanum doping and PEG templating. Process Appl Ceram 8(4):195–202
5. Guan W, Ji F, Xie Z, Li R, Mei N (2015) Preparation and photocatalytic performance of nano-TiO_2 co-doped with iron III and lanthanum III. J Nanomater 2015:1–13
6. Li FB, Li XZ, Hou MF (2004) Photocatalytic degradation of 2-mercaptobenzothiazole in aqueous La^{3+}–TiO_2 suspension for odor control. Appl Catal B 48(3):185–194
7. De la Cruz Romero D, Torres GT, Arévalo JC, Gomez R, Aguilar-Elguezabal A (2010) Synthesis and characterization of TiO_2 doping with rare earths by sol–gel method: photocatalytic activity for phenol degradation. J Sol-Gel Sci Technol 56(3):219–226
8. Li FB, Li XZ, HouMF Cheah KW, Choy WCH (2015) Enhanced photocatalytic activity of Ce^{3+}–TiO_2 for 2-mercaptobenzothiazole degradation in aqueous suspension for odour control. Appl Catal A 285(1–2):181–189
9. Shen XZ, Liu ZC, Xie SM, Guo J (2009) Degradation of nitrobenzene using titaniaphotocatalyst co-doped with nitrogen and cerium under visible light illumination. J Hazard Mater 162(2–3):1193–1198
10. Nasir M, Xi Z, Xing M, Zhang J, Chen F, Tian B, Bagwasi S (2013) Study of synergistic effect of Ce-and S-codoping on the enhancement of visible-light photocatalytic activity of TiO_2. J Phys Chem C 117(18):9520–9528
11. Liqiang J, Xiaojun S, Baifu X, Baiqi W, Weimin C, Honggang F (2004) The preparation and characterization of La doped TiO_2 nanoparticles and their photocatalytic activity. J Solid State Chem 177(10):3375–3382
12. Sun X, Liu H, Dong J, Wei J, Zhang Y (2010) Preparation and characterization of Ce/N-codopedTiO_2 particles for production of H_2 by photocatalytic splitting water under visible light. Catal Lett 135(3–4):219–225
13. Jafari A, Khademi S, Farahmandjou M, Darudi A, Rasuli R (2018) Structural and optical properties of Ce^{3+}-Doped TiO_2 nanocrystals prepared by sol-gel precursors. J Electron Mater 47(11):6901–6908
14. Song S, Tu J, Xu L, Xu X, He Z, Qiu J, Chen J (2008) Preparation of a titanium dioxide photocatalystcodoped with cerium and iodine and its performance in the degradation of oxalic acid. Chemosphere 73(9):1401–1406
15. Luo D, Bi Y, Kan W, Zhang N, Hong S (2011) Copper and cerium co-doped titanium dioxide on catalytic photo reduction of carbon dioxide with water: experimental and theoretical studies. J Mol Struct 994(1–3):325–331
16. Xu J, Ao Y, Fu D (2009) A novel Ce, C-codoped TiO_2 nanoparticles and its photocatalytic activity under visible light. Appl Surf Sci 256(3):884–888
17. Xing MY, Qi DY, Zhang JL, Chen F (2011) One-step hydrothermal method to prepare carbon and lanthanum co-doped TiO2 nanocrystals with exposed 001 facets and their high UV and visible-light photocatalytic activity. Chem A Eur J 17(41):11432–11436
18. Huixian SHI, Zhang T, Hongliang WANG (2011) Preparation and photocatalytic activity of La^{3+} and Eu^{3+} co-doped TiO2 nanoparticles: photo-assisted degradation of methylene blue. J Rare Earths 29(8):746–752
19. Yao S, Jia X, Jiao L, Zhu C, Shi Z (2012) La-doped TiO_2 hollow fibers and their photocatalytic activity under UV and visible light. Indian J Chem 51(8):1049–1056
20. Ndinda E, Park H, Kim KN (2014) Preparation and characterization of cerium doped titanium dioxide nano powder for photocatalyst. Korean J Mater Res 24(1):33–36
21. Yu L, Yang X, He J, He Y, Wang D (2015) One-step hydrothermal method to prepare nitrogen and lanthanum co-doped TiO_2

nanocrystals with exposed 0 0 1 facets and study on their photocatalytic activities in visible light. J Alloy Compd 637:308–314
22. Lan X, Wang L, Zhang B, Tian B, Zhang J (2014) Preparation of lanthanum and boron co-doped TiO_2 by modified sol–gel method and study their photocatalytic activity. Catal Today 224:163–170
23. Chen Q, Jiang D, Shi W, Wu D, Xu Y (2009) Visible-light-activated Ce–Si co-doped TiO_2 photocatalyst. Appl Surf Sci 255(18):7918–7924
24. Kumaresan L, Prabhu A, Palanichamy M, Arumugam E, Murugesan V (2011) Synthesis and characterization of Zr^{4+}, La^{3+} and Ce^{3+} doped mesoporous TiO_2: evaluation of their photocatalytic activity. J Hazard Mater 186(2–3):1183–1192
25. Huang Y, Cao JJ, Kang F, You SJ, Chang CW, Wang YF (2017) High selectivity of visible-light-driven La-doped TiO_2 photocatalysts for NO removal. Aerosol Air Qual Res 17(10):2555–2565
26. Tobaldi DM, Pullar RC, Škapin AS, Seabra MP, Labrincha JA (2014) Visible light activated photocatalyticbehaviour of rare earth modified commercial TiO_2. Mater Res Bull 50:183–190
27. Nasir M, Bagwasi S, Jiao Y, Chen F, Tian B, Zhang J (2014) Characterization and activity of the Ce and N co-doped TiO_2 prepared through hydrothermal method. Chem Eng J 236:388–397
28. Umar K, Haque MM, Muneer M, Harada T, Matsumura M (2013) Mo, Mn and La doped TiO_2: synthesis, characterization and photocatalytic activity for the decolourization of three different chromophoric dyes. J Alloys Compd 578:431–438
29. Tong T, Zhang J, Tian B, Chen F, He D, Anpo M (2007) Preparation of Ce–TiO_2 catalysts by controlled hydrolysis of titanium alkoxide based on esterification reaction and study on its photocatalytic activity. J Colloid Interface Sci 315(1):382–388
30. Khodadadi B (2016) Facile sol–gel synthesis of Nd, Ce-codoped TiO_2 nanoparticle using starch as a green modifier: structural, optical and photocatalytic behaviors. J Sol-Gel Sci Technol 80(3):793–801
31. He Z, Xu X, Song S, Xie L, Tu J, Chen J, Yan BA (2008) visible light-driven titanium dioxide photocatalystcodoped with lanthanum and iodine: an application in the degradation of oxalic acid. J Phys Chem C 112(42):16431–16437
32. Quan X, Tan H, Zhao Q, Sang X (2007) Preparation of lanthanum-doped TiO_2 photocatalysts by coprecipitation. J Mater Sci 42(15):6287–6296
33. Ellappan P, Miranda LR (2014) Synthesis and characterization of cerium doped titanium catalyst for the degradation of nitrobenzene using visible light. Int J Photoenergy 2014:1–9
34. Aman N, Satapathy PK, Mishra T, Mahato M, Das NN (2012) Synthesis and photocatalytic activity of mesoporous cerium doped TiO_2 as visible light sensitive photocatalyst. Mater Res Bull 47(2):179–183
35. Choudhury B, Borah B, Choudhury A (2012) Extending photocatalytic activity of TiO_2 nanoparticles to visible region of illumination by doping of cerium. Photochem Photobiol 88(2):257–264
36. Wei CH, Tang XH, Liang JR, Tan SY (2007) Preparation, characterization and photocatalytic activities of boron-and cerium-codoped TiO_2. J Environ Sci 19(1):90–96
37. Liu C, Tang X, Mo C, Qiang Z (2008) Characterization and activity of visible-light-driven TiO_2 photocatalystcodoped with nitrogen and cerium. J Solid State Chem 181(4):913–919
38. Jiang YF, Chen YY, Zhang B, Fen YQ (2016) N, La Co-doped TiO_2 for use in low-temperature-based dye-sensitized solar cells. J Electrochem Soc 163(10):F1133–F1138
39. Singh I, Birajdar B (2019) Effective La-Na Co-Doped TiO_2 nanoparticles for dye adsorption: synthesis. Charact Study Adsorpt Kinet Nanomater 9(3):400
40. Hua C, Dong X, Wang X, Xue M, Zhang X, Ma H (2014) Enhanced photocatalytic activity of w-doped and w-la-codoped TiO_2 nanomaterials under simulated sunlight. J Nanomater 2014:943796
41. Lei XF, Chen C, Li X, Xue XX, Yang H (2016) Characterization and photocatalytic performance of La and C co-doped anatase TiO_2 for photocatalytic reduction of Cr (VI). Sep Purif Technol 161:8–15